THE JOURNAL OF BIOLOGICAL CHEMISTRY
Vol. 275, No. 12, Issue of March 24, pp. 8680–8685, 2000
Printed in U.S.A.

Nuclear Magnetic Resonance Solution Conformation of α-Conotoxin AuIB, an $\alpha_3\beta_4$ Subtype-selective Neuronal Nicotinic Acetylcholine Receptor Antagonist*

(Received for publication, October 4, 1999, and in revised form, December 17, 1999)

Jee-Hyun Cho‡, K. Hun Mok‡, Baldomero M. Olivera§, J. Michael McIntosh§¶, Kyu-Hwan Park‡, and Kyou-Hoon Han‡‖

From the ‡Protein Engineering Laboratory, Korea Research Institute of Bioscience and Biotechnology, Yusong, Taejon 305-600, Republic of Korea and Departments of §Biology and ¶Psychiatry, University of Utah, Salt Lake City, Utah 84112

The neuronal nicotinic acetylcholine receptors constitute a highly diverse group, with subtypes consisting of pentameric combinations of α and β subunits. α-Conotoxins are a homologous series of small peptides that antagonize these receptors. We present the three-dimensional solution structure of α-conotoxin AuIB, the first 15-residue α-conotoxin known to selectively block the $\alpha_3\beta_4$ nicotinic acetylcholine receptor subtype. The pairwise backbone and heavy-atom root mean square deviation for an ensemble of 20 structures are 0.269 and 0.720 Å, respectively. The overall fold of α-conotoxin AuIB closely resembles that of the α4/7 subfamily α-conotoxins. However, the absence of Tyr[15], normally present in other α4/7 members, results in tight bending of the backbone at the C terminus and effectively renders Asp[14] to assume the spatial location of Tyr[15] present in other neuronal α4/7 α-conotoxins. Structural comparison of α-conotoxin AuIB with the $\alpha_3\beta_2$ subtype-specific α-conotoxin MII shows different electrostatic surface charge distributions, which may be important in differential receptor subtype recognition.

The α-conotoxins are small neuropharmacologically active peptides of *Conus* origin that antagonize the nicotinic acetylcholine receptor (nAChR)[1] (1). The natural diversity of biosynthesized conotoxin peptides has led to the classification of a wide spectrum of disulfide-bridged peptides, which attack various ligand and ion-gated channels and receptors (1). The nicotinic acetylcholine receptors exhibit considerable diversity in their own right because of the different compositions found in the pentameric subunits constituting each nAChR subtype (2). Although the mammalian neuromuscular subtype comprises $(\alpha_1)_2\beta\gamma\delta$ or $(\alpha_1)_2\beta\varepsilon\delta$ subunits, the neuronal subtypes are comparatively more diverse with their hetero- or homopentameric combinations of α ($\alpha_2 \sim \alpha_9$) or β ($\beta_2 \sim \beta_4$) subunits (3, 4). The general conotoxin strategy of diversification is "combinatorial" (5), in which amino acid residues are varied within a given disulfide framework to specifically and selectively bind various subtypes of the target channel or receptor. For the case of α-conotoxins, target selectivity is essentially defined depending on which subunit interface of the nAChR (*e.g.* α_1/γ, α_1/δ, and α_3/β_2) each individual α-conotoxin preferentially binds to (1). Highly selective α-conotoxins that permit differential blocking of diverse nAChR subtypes have served as effective tools in studying these receptors (1).

Of recent particular interest are the α-conotoxins that act on neuronal nAChRs. For example, α-conotoxin AuIB specifically targets the $\alpha_3\beta_4$ subtype (6), whereas α-conotoxin MII selectively blocks the $\alpha_3\beta_2$ subtype (7). On the other hand, α-conotoxin ImI, the smallest of all α-conotoxins and distinct because of its α4/3 disulfide framework[2], is a specific antagonist of the homomeric α_7 subtype (8). In addition, other neuronal α-conotoxins such as PnIA (9), PnIB (9), and EpI (10) that are less selective to a particular nAChR subtype have also been identified (Table I).

As shown in Table I, most neuronal α-conotoxins belong to the α4/7 subfamily, in which the amino acid sequence varies within disulfide bridge-enclosed loops of 4 and 7 residues. Interestingly, α-conotoxin EI, unique in its specificity for the α_1/δ subunit interface in *Torpedo* neuromuscular nAChR, belongs to the same α4/7 subfamily (11). The recent increase in the understanding of these conotoxins has been attributable to the advances in the structural characterization of these molecules. High-resolution three-dimensional structures of α4/7 subfamily α-conotoxins PnIA (12), PnIB (13), MII (14, 15), and [Tyr[15]]EpI (16) show that, when backbone-superimposed, their backbone fold is extremely similar. The recently solved NMR structure of α-conotoxin EI also has the same overall molecular fold as the α4/7 neuronal α-conotoxins[3] despite the variation in its sequence both within the disulfide loops and at the N terminus (Table I). These observations reaffirm that conotoxins are based on common three-dimensional scaffolds and that their subtype selectivity is conferred through sequence variation of a selected number of residues (5).

Through structural elucidation of these highly selective α-conotoxins and their analogs (17, 18), we have been using the reverse-mapping approach first to identify receptor subtype specific determinants in the ligands and second to indirectly probe the regions in nAChR responsible for binding agonists

* This research was supported in part by Grant NB0980 from the Ministry of Science and Technology, Korea. The costs of publication of this article were defrayed in part by the payment of page charges. This article must therefore be hereby marked "*advertisement*" in accordance with 18 U.S.C. Section 1734 solely to indicate this fact.

The atomic coordinates and structure factors (code 1DG2) have been deposited in the Protein Data Bank, Research Collaboratory for Structural Bioinformatics, Rutgers University, New Brunswick, NJ (http:wwwresb.org1).

‖ To whom correspondence should be addressed: Protein Engineering Laboratory, Korea Research Institute of Bioscience and Biotechnology, Yusong P.O. Box 115, Taejon 305-600, Republic of Korea. Tel.: 82-42-860-4250; Fax: 82-42-860-4259; E-mail: khhan@biotech5.kribb.re.kr.

[1] The abbreviations used are: nAChR, nicotinic acetylcholine receptor; NOE, nuclear Overhauser effect; NOESY, nuclear Overhauser effect spectroscopy; COSY, correlation spectroscopy; RMSD, root mean square deviation.

[2] The α-conotoxins are additionally grouped according to the number of amino acid residues enclosed within each disulfide loop. Loop sizes of four residues in the first loop and seven in the second are denoted as α4/7. Other subfamilies include α3/5 and α4/3.

[3] K.-H. Park, J. E. Suk, R. Jacobsen, W. R. Gray, J. M. McIntosh, B. M. Olivera, and K. Han, manuscript in preparation.

TABLE I
Amino acid sequences of α4/7 subfamily α-conotoxins that target neuronal nAChR

All listed α-conotoxins are neuronal toxins except EI, which is a neuromuscular toxin. The asterisk indicates an amidated C terminus.

Name	Sequence	Specificity	Reference
AuIB	GCCSYPPCFATNP-DC*	$\alpha_3\beta_4$	6
AuIC	GCCSYPPCFATNSGYC*	$\alpha_3\beta_4$	6
AuIA	GCCSYPPCFATNSDYC*	$\alpha_3\beta_4$	6
MII	GCCSNPVCHLEHSNLC*	$\alpha_3\beta_2$	7
PnIA	GCCSLPPCAANNPDYC*	$\alpha_3\beta_2$	36
PnIB	GCCSLPPCALSNPDYC*	α_7	36
EpI	GCCSDPRCNMNNPDYC*	$\alpha_3\beta_2$, $\alpha_3\beta_4$	10
ImI[a]	GCCSDPRCA--W-R-C*	α_7	17, 18
EI	RDOCCYHPTCNMSNPQIC*	$\alpha_1\delta$	11

[a] α-Conotoxin ImI is an α4/3 conotoxin.

and antagonists. We hereby present the high-resolution solution structure of α-conotoxin AuIB that has a unique $\alpha_3\beta_4$ nAChR subtype selectivity (6). $\alpha_3\beta_4$-like receptors are believed to be important in peripheral ganglionic transmission and centrally mediated norepinephrine release. α-Conotoxin AuIB inherently lacks Tyr^{15} found in other α4/7 members such as α-conotoxins PnIA, PnIB, EpI, and even AuIA and AuIC (Table I). Of the three α-conotoxin AuIs found in *Conus aulicus* (6), α-conotoxin AuIB is the best characterized from a functional standpoint and has thus been chosen for detailed structural analysis by NMR. Structural comparison of α-conotoxin AuIB with other neuronal α-conotoxins should provide useful insight into important nAChR subtype determinants, in particular, those that discriminate the β_2 and β_4 subunits.

EXPERIMENTAL PROCEDURES

Peptide Synthesis and Purification—α-Conotoxin AuIB was synthesized using solid-phase chemistry and purified to homogeneity as described previously (6).

NMR Spectroscopy—Samples for NMR studies were prepared in 90% H_2O and 10% ^2H_2O or 100% ^2H_2O, pH 4.1, with a final sample concentration of 6 mM. All NMR experiments were performed using a Varian UNITY INOVA 600 spectrometer at 278 and 298 K. Solvent suppression was carried out using selective, low-powered irradiation of the water resonance during a relaxation delay of 1.5 s. All resonances were referenced to a residual water signal (4.76 ppm at 298 K). Mixing times of 200–400 ms for NOESY and 150 ms for rotating frame NOESY experiments were used. For total correlation spectroscopy experiments (19), a 75-ms mixing time was used. $^3J_{HNH\alpha}$ coupling constants for the backbone torsion angle were measured using phase-sensitive double-quantum-filtered two-dimensional COSY experiments (20). Primitive exclusive COSY (21) was performed in 100% ^2H_2O to measure the $^3J_{\alpha\beta}$coupling constants, which were used in conjunction with the $d_{N\beta}$ NOEs to provide χ^1 torsion angles. Spectral widths were 7.0 kHz in both dimensions. Typical two-dimensional data consisted of 2048 complex points in the t_2 dimension and 256 complex t_1 increments. Data acquisition, sequential assignments, and spectral interpretation were performed on SPARCstation IPX and Ultra 1 Creator workstations (Sun Microsystems) running VnmrX 5.3B software (Varian Associates)

Computation of Structures—Two-dimensional NMR data were processed using Felix 95.0 and Insight II 97.0 (Biosym/MSI) on Indigo2 xL or Indy workstations (Silicon Graphics). NOE interproton distance constraints were derived primarily from the NOESY spectrum obtained at 278K with a mixing time of 200 ms. Before Fourier transformation, free induction decays were reconstructed using linear prediction, apodized with a 60° sine bell-squared window function in both dimensions, and baseline corrected using the FLATT algorithm (22). NOE cross-peak volumes were measured and converted into upper bounds of interproton distances using the distance of 1.8 Å as a reference for nonoverlapping geminal β-proton cross-peaks. Appropriate pseudoatom allowances of 1.5–2.5 Å were given to constraints. Dihedral angle restraints were inferred from $^3J_{HNH\alpha}$coupling constants and were centered on $-120° \pm 30°$ for $^3J_{HNH\alpha} > 8$ Hz and $-60° \pm 30°$ for $^3J_{HNH\alpha} < 6$ Hz. Side chain χ^1 torsion angles measured from primitive exclusive COSY experiments were also incorporated in combination with the sequential $d_{\alpha\beta}$ NOE for stereospecifically assigned β-methylene protons. A total of 156, including 13 long-range and 25 medium-range, distance constraints, together with eight ϕ and two χ^1 torsion angles were input for the computation of structures.

Preliminary structures were generated using DGII (23), NMRchitect, and Insight II 97.0. An extended molecule with two disulfide bridges and a formal charge of zero was constructed. The potentials and partial charges were assigned using the consistent valence force field (24) and used throughout the computations. Full relaxation matrix analysis using MARDIGRAS version 3.2 (25) was performed on DGII-generated structures as initial model structures. The three-site jump model for intra- and inter-residue distances was chosen, and the noise level was estimated to be 50% of the un-normalized absolute value of the smallest peak. The rotational correlation time was estimated to be 1.0 ns.

Structures were refined with restrained molecular dynamics calculations with Discover 2.9.7 (Biosym/MSI) and Insight II 95.0. A simulated annealing schedule based on well established protocols (26) was generated and run. The 68-ps protocol consisted of dynamics at 1000 K (50 ps), followed by gradual temperature cooling from 1000 to 300 K (incremental temperature decrease of 100 K each over 18 ps) with staggered geometric increases of NOE, covalent term, and nonbonded force constants. During the final dynamics step at 300 K and subsequent minimization steps, a modified restraint file with decreased force constants for side chain interproton distances was used to allow further conformational dynamics. Energy minimization was performed 2-fold, first with a quadratic potential and then with a Lennard-Jones nonbonded potential. A total of 50 simulated annealing rounds were run.

Assessment of Structure Quality and Visualization of Structures—The R_a and R_b factors (27) were calculated using CORMA version 5.2 (28) for the final ensemble of 20 structures. In addition, the stereochemistry of the computed structures were analyzed with PROCHECK version 3.5 (29). The three-dimensional display of structures was performed either with Insight II 97.0 (Biosym/MSI) or GRASP version 1.3.6 (30).

RESULTS

Resonance Assignment and Secondary Structure—The complete ^1H resonance assignment for α-conotoxin AuIB was achieved in a straightforward manner using double-quantum-filtered two-dimensional COSY, total correlation spectroscopy, and NOESY and rotating frame NOESY spectra following the standard sequential assignment procedure (31). Initial assignment of the amino acids was made along the NH resonances in double-quantum-filtered two-dimensional COSY and total correlation spectroscopy spectra. Apart from Thr^{11}, where the Hα and Hβ protons showed overlapping, all Hα and side chain protons were unambiguously resolved, permitting the tracing of sequential Hα-NH(i + 1) connectivities. The connectivity was broken at three proline residues (Pro^6, Pro^7, and Pro^{13}), for which resonance assignment was achieved using strong $d_{\alpha\delta}(Tyr^5, Pro^6)$, $d_{\alpha\delta}(Pro^6, Pro^7)$, and $d_{\alpha\delta}(Asn^{12}, Pro^{13})$ cross-peaks that indicate all prolines have the trans conformation. Fig. 1 is a summary of sequential and medium-range NOEs used for the resonance assignment, the $^3J_{HNH\alpha}$ values, the temperature coefficients for NH protons ($\Delta\delta_{NH}$), and chemical shift indices (32). The stretches of $d_{\alpha N}(i, i + 3)$, $d_{\alpha\beta}(i, i + 3)$, and $d_{\alpha N}(i, i + 4)$ NOEs between Pro^6 and Asn^{12} makes the presence of an α-helix evident before the detailed structure calculations.

Structure Calculations—Fig. 2 shows the superposition of a final ensemble of 20 lowest energy structures. The backbone and heavy atom RMSD values for the entire chain are 0.269 and 0.720 Å, respectively. Omitting the flexible N-terminal Gly^1 residue, the backbone RMSD value improves considerably to 0.092 Å, with the heavy atom RMSD being 0.707 Å. As shown in Table II, overall structural statistics concerning experimental restraints, covalent geometry, and structural convergence for α-conotoxin AuIB are extremely good. When subject to quality evaluation by PROCHECK (29), backbone dihedral angles of all non-Gly and non-Pro residues were found to reside within the most favored region of the Ramachandran plot (Table II).

Three-dimensional Structure of α-Conotoxin AuIB—The backbone fold of α-conotoxin AuIB has the shape of the Greek

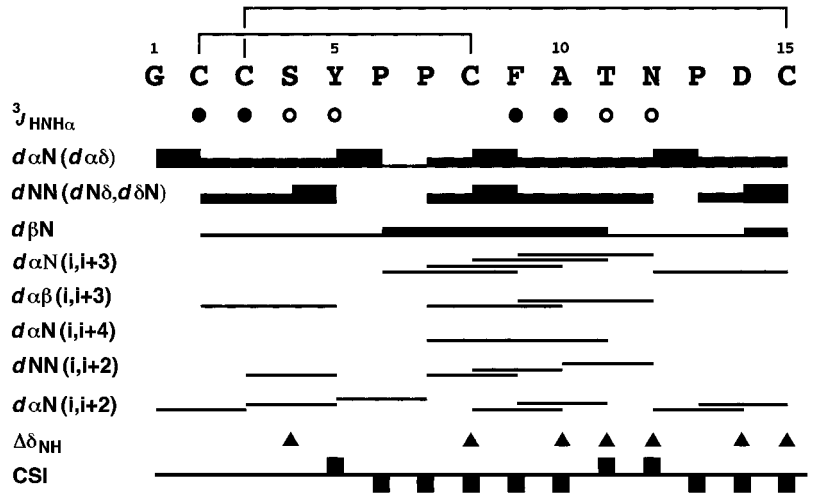

FIG. 1. **Summary of sequential and medium-range NOE connectivities, $^3J_{HNH\alpha}$ coupling constants, NH temperature coefficients ($\Delta\delta_{NH}$), and chemical shift indices for α-conotoxin AuIB.** The thickness of the *bars* is proportional to the NOE intensity, classified as strong, medium, or weak. *Filled circles* denote $^3J_{HNH\alpha}$ values of <6.0 Hz; *open circles* indicate $^3J_{HNH\alpha}$ values of >8.0 Hz. For the NH temperature coefficients, *filled triangles* denote $\Delta\delta_{NH}$ <3 ppb/K. Chemical shift index values of +1, 0, and −1 are represented as above, no indication, and below the *horizontal line*, respectively.

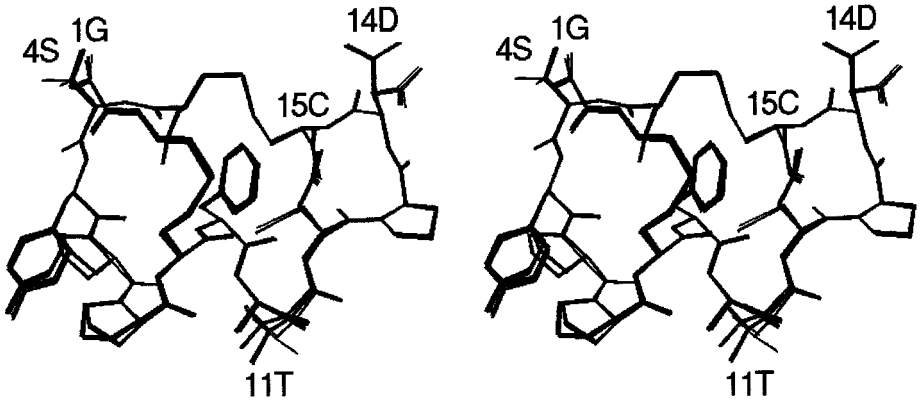

FIG. 2. **Stereo view of the 20 final structures of α-conotoxin AuIB superimposed over backbone atoms (N, C^α, C′, and O) of residues 2–15.** Selected residues are labeled.

TABLE II
NMR structure determination statistics of α-conotoxin AuIB for an ensemble of 20 structures

RMS deviations from Experimental restraints[a]	
Interproton distances (Å)	0.0222 ± 0.0019
Torsion angle violation (°)	0.3663 ± 0.0311
Ramachandran plot statistics	
Residues in most favored region (%)	100.0
Residues in additionally allowed region (%)	0.0
Residues in generously allowed region (%)	0.0
Residues in disallowed region (%)	0.0
Ensemble *R* factors[a,b]	
R_a	0.425 ± 0.005
R_b	0.139 ± 0.006
RMS deviations from the average structure	
Residues 2–15	
Backbone atoms[c]/heavy atoms (Å)	0.092/0.707
Residues 1–15	
Backbone atoms/heavy atoms (Å)	0.269/0.720

[a] Values are means ± S.D.
[b] R_a and R_b values are computed as defined in Ref. 27.
[c] Backbone atoms are N, C^α, C′, and O.

letter ω, which is characteristic of all α4/7 α-conotoxins (Fig. 3). The N-terminal Cys^2-Tyr^5 residues constitute a type I β-turn. This is followed by a two-turn α-helix (Tyr^5-Asn^{12}), which forms the bottom portion of the ω fold. The C terminus (Asn^{12}-Cys^{15}) forms a bend at Pro^{13} to properly complete the Cys^3-Cys^{15} disulfide bridge. Of the two disulfide bridges present in α-conotoxin AuIB, χ^1 angles for the Cys^3-Cys^{15} pair were determined experimentally and used to calculate a left-handed spiral conformation. The final ensemble of the Cys^2-Cys^8 disulfide bridge also converged well to a single, left-handed form. These disulfide conformations are in good agreement with those observed in high-resolution x-ray structures of other α4/7 members such as α-conotoxins PnIA (12) PnIB (13) and [Tyr^{15}]EpI (16). As shown in Fig. 3, the inherent absence of a tyrosine between Asp^{14} and Cys^{15} in α-conotoxin AuIB does not influence the overall conformation of the Cys^3-Cys^{15} disulfide bridge to any appreciable extent. However, this deletion renders the local backbone fold near Asp^{14} and Cys^{15} in α-conotoxin AuIB noticeably different from that in other α4/7 members (see Fig. 5*A*). Two consecutive β turns found at their C termini of other α4/7 members are absent in α-conotoxin AuIB.

DISCUSSION

Structural Comparison with Other α4/7 α-Conotoxins—The α4/7 subfamily of α-conotoxins share a common ω backbone fold, as demonstrated in Fig. 3. The pairwise backbone RMSDs of α-conotoxin AuIB with other α4/7 members are 0.97 Å with MII (Protein Data Bank file name, 1M2C), 0.61 Å with PnIA (1PEN), 0.70 Å with PnIB (1AKG), and 0.52 Å with [Tyr^{15}]EpI (1A0M). A common backbone scaffold shared by the α4/7 members would presumably provide an efficient means for combinatorial presentation of functional side chain moieties that specifically interact with the receptor (5). As shown in Table I, when excluding the neuromuscular-targeting α-conotoxin EI, the N-terminal disulfide loop of all α4/7 subfamily members contains an SνP(P/V) sequence (ν is a variable residue) except for α-conotoxin EpI, which is not particularly specific for one subtype. Ligand binding to the α subunit of nAChR is known to be primarily mediated by hydrophobic aromatic interactions (33–35). Surface characteristics of the putative SνP(P/V) region in α4/7 α-conotoxins shown below by GRASP suggest that the mostly hydrophobic SνP(P/V) sequence may represent a common α_3 subunit recognition face in neuronal α4/7 members.

The variability in sequence across the C-terminal seven-residue loop is greater, in particular, for the first three residues. The amino acid types for the last four residues in the

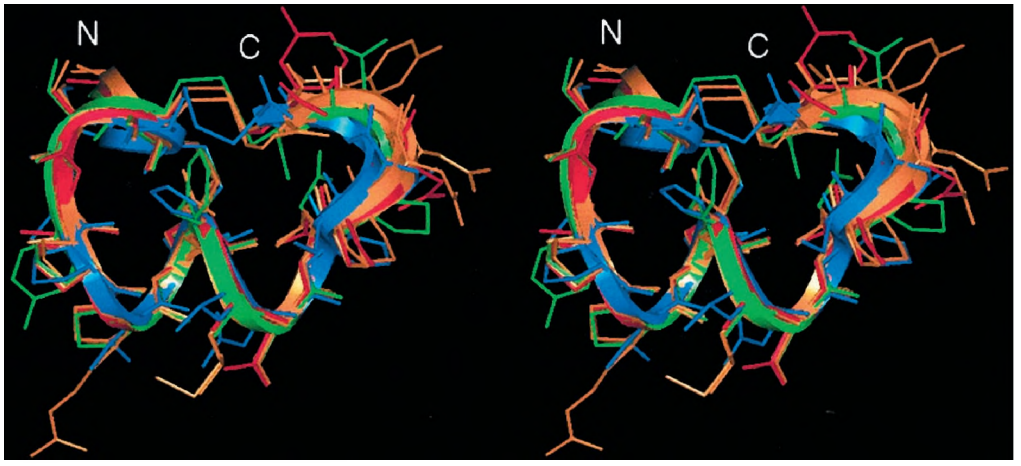

FIG. 3. **Ribbon diagrams of five superimposed structures of neuronal α4/7 subfamily α-conotoxins AuIB (*green*; this work), MII (*blue*; Protein Data Bank file name, 1M2C), PnIA (*yellow*; 1PEN), PnIB (*orange*; 1AKG), and EpI (*red*; 1A0M).** *N* and *C*, N and C termini, respectively. The former two were determined by NMR, whereas the latter three were determined by x-ray crystallography.

same loop can reasonably be represented by (P/S)(D/N)(Y/L)C. Because this C-terminal sequence is shared, it is unlikely that this region is responsible for the different nAChR subtype specificities exhibited by each toxin. For example, both α-conotoxins AuIA and AuIC possess Tyr^{15} (Table I), yet their $\alpha_3\beta_4$ subtype selectivity is only slightly weaker than α-conotoxin AuIB (6). Therefore, Gly^{14} in α-conotoxin AuIC and the missing Tyr^{15} α-conotoxin AuIB are not likely to be essential for defining the $\alpha_3\beta_4$ subtype selectivity. As noted above, the missing Tyr^{15} from the PDYC sequence in α-conotoxin AuIB results in a different local backbone C-terminal fold from other α4/7 members. Using α-conotoxin PnIA as a reference, divergence in the α-conotoxin AuIB backbone trace begins with Pro^{13}, where the Pro rings of both α-conotoxins PnIA and AuIB display perpendicular orientations. A strong backbone bend follows, placing the Asp^{14} Cα of α-conotoxin AuIB closer to the Tyr^{15} Cα than the Asp^{14} Cα of α-conotoxin PnIA (Fig. 3). It remains to be seen whether the observed spatial shift of the Asp^{14} side chain contributes to the higher antagonistic activity of α-conotoxin AuIB than AuIA/C.

Fig. 4 shows electrostatic potential surfaces generated by GRASP (30) for α-conotoxins AuIB, PnIA, [Tyr^{15}]EpI, and MII. The viewing direction is kept same as that in Fig. 3. The positively charged N terminus (*upper left region*) is observed for all four toxins. The *upper right* hydrophobic bulge corresponds to Tyr^{15} of α-conotoxins PnIA and [Tyr^{15}]EpI or Leu^{15} in α-conotoxin MII. Note that the negatively charged Asp^{14} of α-conotoxin AuIB is found at the corresponding location. A deep cleft is observed in the left side of MII, but the corresponding site in α-conotoxins AuIB and EpI is filled with Tyr^5 and Asp^5, respectively. The conspicuous hydrophobic bulge formed by Leu^{10} in the middle of MII is absent in other α4/7 members, suggesting that Leu^{10} in MII is important for its β_2 subunit selectivity (see below). Significance of the residue at position 10 in the α4/7 subfamily is further illustrated by the following observation. α-Conotoxins PnIA and PnIB differ in only two positions, yet their selectivities are markedly different (Table I). Interestingly, substituting Ala^{10} by Leu turns the $\alpha_3\beta_2$ subtype-specific PnIA into an α_7 subtype-specific toxin, suggesting that only position 10 is necessary to differentiate the two toxins (1).

Comparison of α-Conotoxins AuIB and MII—As shown in Fig. 5, more specific comparison can be made between two members of the α4/7 subfamily, AuIB and MII, because the former is highly selective toward the $\alpha_3\beta_4$ nAChR subtype, whereas the latter is selective for the $\alpha_3\beta_2$ subtype. MII is

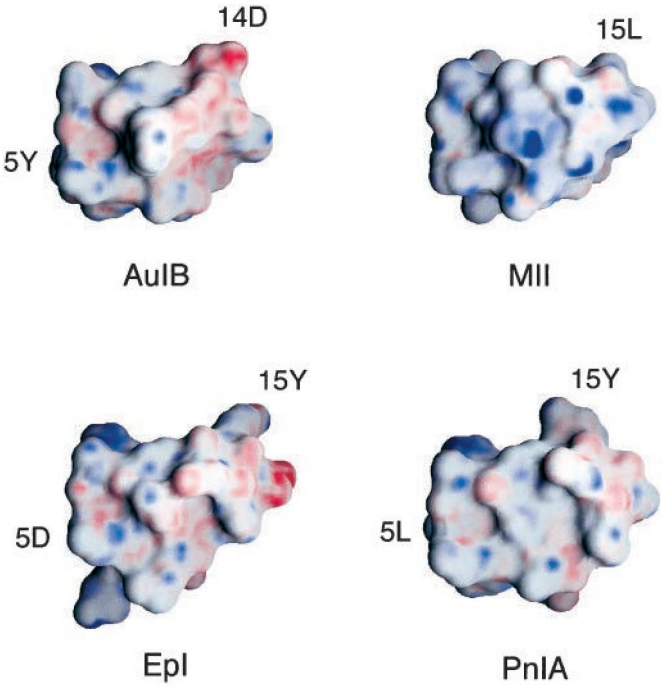

FIG. 4. **Electrostatic surface potential representations of α-conotoxins AuIB, MII, [Tyr^{15}]EpI, and PnIA.** The structures are oriented in the same direction as in Fig. 3 to place the N terminus on the *upper left* and the C terminus on the *upper right*. Some selected residues are labeled. Regions of the surface with electrostatic potentials greater than +15kT, equal to 0, and less than −15kT are *blue*, *white*, and *red*, respectively. The atomic charges were taken from the consistent valence force field (24), and the calculations and generation of the diagram were performed with GRASP (30).

chosen as the $\alpha_3\beta_2$ subtype-specific toxin, because α-conotoxin PnIA, another $\alpha_3\beta_2$-targeting toxin, is much less selective than α-conotoxin MII toward the same receptor subtype (1). At present, two different NMR structures of MII are available, one determined in aqueous solution (Ref. 15; 1M2C) and the other in 30% 2,2,2-trifluoroethanol (Ref. 16; 1MII). Because the structure of α-conotoxin AuIB was determined in aqueous solution without 2,2,2-trifluoroethanol, structural comparisons were made with the former. In fact, backbone comparisons of α-conotoxin AuIB with both structures indicate that the former agrees better when superimposed (pairwise RMSDs, 0.97 Å for 1M2C and 1.29 Å for 1MII). Note in Fig. 5*A* the aforementioned

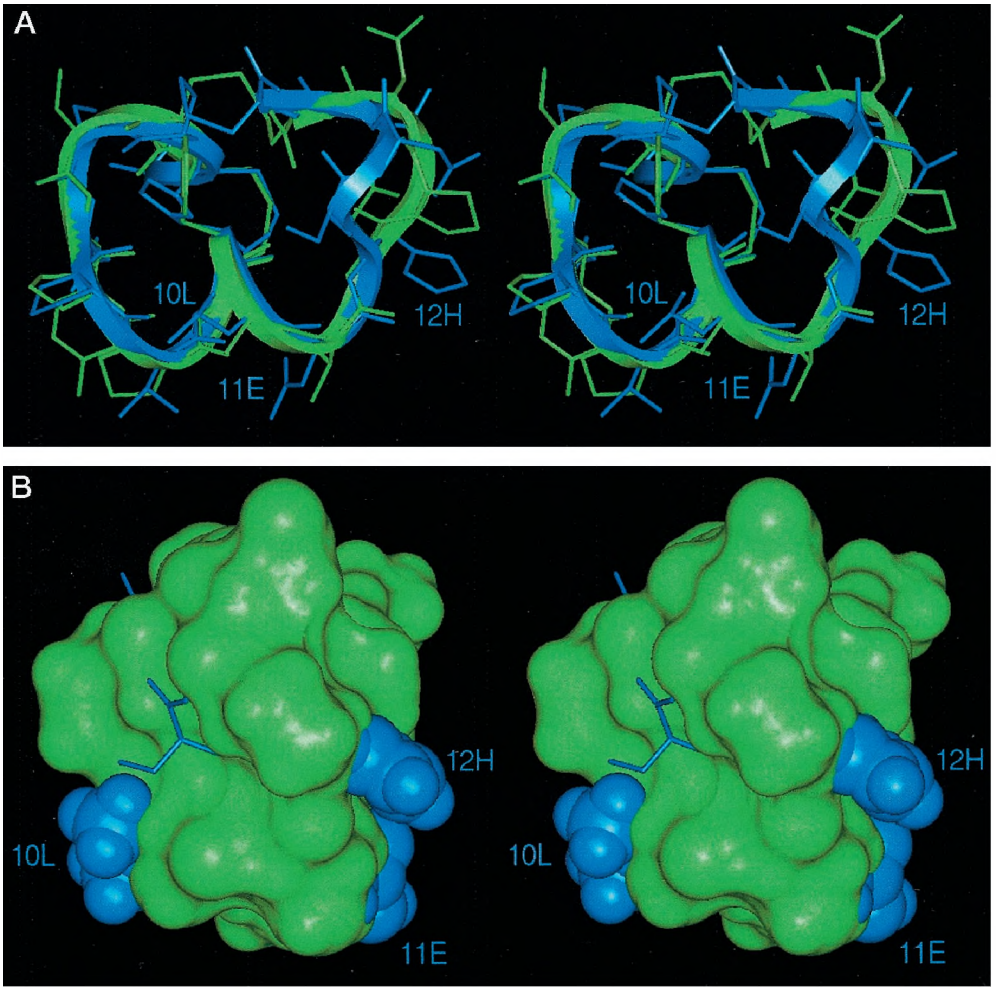

FIG. 5. **Structural comparison between α-conotoxins AuIB (*green*) and MII (*blue*).** *A*, ribbon diagrams showing the difference in the backbone near residues 13–15. *B*, Connolly surface comparison between two toxins. Three residues of MII are exposed out of the AuIB surface and labeled. The viewing direction differs by 90° from *A*.

local backbone difference near residues 13–15 between α-conotoxins MII and AuIB. This difference is also clearly visible when the structure of α-conotoxin MII determined in 2,2,2-trifluoroethanol is used for comparison, because the structures of α-conotoxin MII in two solvent conditions are essentially the same.

If a comparative surface exposure approach previously used for α-conotoxin EI[3] is applied to compare the two toxins (Fig. 5*B*), three residues of α-conotoxin MII become exposed out of the AuIB surface, Leu^{10}, Glu^{11}, and His^{12}. The former two were shown to be important for distinguishing neuromuscular from neuronal nAChR.[3] Note that GRASP analysis above suggested Leu^{10} to be important for the β_2 subunit selectivity of α-conotoxin MII. The third residue, His^{12}, is unique in that no other α4/7 members have such an aromatic bulky residue at the same position (Table I). Intriguingly, His^{12} is buried underneath bulky side chains of Arg^9 and His^{10} of neuromuscular α-conotoxin GI and hence is not surface-exposed when α-conotoxins GI and MII are superimposed.[3] These results suggest that His^{12} in α-conotoxin MII is important for distinguishing two different neuronal nAChR subtypes, $\alpha_3\beta_4$ and $\alpha_3\beta_2$, but makes no contribution to discriminating the neuronal nAChR subtype against the neuromuscular subtype.

The surface-exposed Ser^{13} of α-conotoxin MII is not considered important, because it stays outside of the AuIB surface because of the different local backbone topology pointed out earlier. This residue is not exposed if α-conotoxin MII is superimposed with other α4/7 members such as PnIA/B or EpI. Rather interesting is that there are no prominently protruding AuIB residues out of the MII surface, except for the hydroxyl tip of Tyr^5 and the carboxylate side chain of Asp^{14}. An alanine-scanning study on α-conotoxin AuIB should provide answers on the significance of these residues for the β_4 subtype specificity.

The structural details of α-conotoxin binding with nAChR are currently incomplete. Despite the overall differences or local similarity among these toxins, it is certainly difficult to unambiguously define the respective subtype selectivities based only on such structural features (18). Binding determinants within the α4/7 subfamily are subtle and may not be immediately discernible, as can be judged from the fact that the overall structural fold is same, whereas only types of amino acids are varied. Hence, structural comparison of different α-conotoxins needs to be augmented by additional information from site-directed mutagenesis and chimeric receptor engineering (3, 36, 37). Cumulative results support that both α and non-α subunits of the neuronal nAChR contribute to the binding of agonists and antagonists (38–42), although the extent of contribution from different subunits to ligand binding needs to be better-characterized.

Acknowledgments—We thank Dong-Ho Choung for technical assistance in carrying out the NMR experiments. We also thank Prof. Thomas L. James for the CORMA and MARDIGRAS software packages and Prof. Barry Honig and Dr. Anthony Nicholls for kindly providing the GRASP software.

REFERENCES

1. McIntosh, J. M., Santos, A. D., and Olivera, B. M. (1999) *Annu. Rev. Biochem.* **68,** 59–88
2. Karlin, A., and Akabas, M. H. (1995) *Neuron* **15,** 1231–1244
3. Sargent, P. B. (1993) *Annu. Rev. Neurosci.* **16,** 403–443
4. Lindstrom, J. (1997) *Mol. Neurobiol.* **15,** 193–222
5. Olivera, B. M., Hillyard, D. R., Marsh, M., and Yoshikami, D. (1995) *Trends Biotechnol.* **13,** 422–426
6. Luo, S., Kulak, J. M., Cartier, G. E., Jacobsen, R. B., Yoshikami, D., Olivera, B. M., and McIntosh, J. M. (1998) *J. Neurosci.* **18,** 8571–8579
7. Cartier, G. E., Yoshikami, D., Gray, W. R., Luo, S., Olivera, B. M., and McIntosh, J. M. (1996) *J. Biol. Chem.* **271,** 7522–7528
8. Johnson, D. S., Martinez, J., Elgoyhen, A. B., Heinemann, S. F., and McIntosh, J. M. (1995) *Mol. Pharmacol.* **48,** 194–199
9. Fainzilber, M., Hasson, A., Oren, R., Burlingame, A. L., Gordon, D., Spira, M. E., and Zlotkin, E. (1994) *Biochemistry* **33,** 9523–9529
10. Loughnan, M., Bond, T., Atkins, A., Cuevas, J., Adams, D. J., Broxton, N. M., Livett, B. G., Down, J. G., Jones, A., Alewood, P. F., and Lewis, R. J. (1998) *J. Biol. Chem.* **273,** 15667–15674
11. Martinez, J. S., Olivera, B. M., Gray, W. R., Craig, A. G., Groebe, D. R., Abramson, S. N., and McIntosh, J. M. (1995) *Biochemistry* **34,** 14519–14526
12. Hu, S.-H., Gehrmann, J., Guddat, L. W., Alewood, P. F., Craik, D. J., and Martin, J. L. (1996) *Structure* **4,** 417–423
13. Hu, S.-H., Gehrmann, J., Alewood, P. F., Craik, D. J., and Martin, J. L. (1997) *Biochemistry* **36,** 11323–11330
14. Shon, K.-J., Koerber, S. C., Rivier, J. E., Olivera, B. M., and McIntosh, J. M. (1997) *Biochemistry* **36,** 15693–15700
15. Hill, J. M., Oomen, C. J., Miranda, L. P., Bingham, J.-P., Alewood, P. F., and Craik, D. J. (1998) *Biochemistry* **37,** 15621–15630
16. Hu, S.-H., Loughnan, M., Miller, R., Weeks, C. M., Biessing, R. H., Alewood, P. F., Lewis, R. J., and Martin, J. L. (1998) *Biochemistry* **37,** 11425–11433
17. Han, K., Hwang, K. J., Kim, S. M., Kim, S. K., Gray, W. R., Olivera, B. M., River, J., and Shon, K. J. (1997) *Biochemisty* **37,** 1669–1677
18. Mok, K. H., and Han, K. (1999) *Biochemisty* **38** 11895–11904
19. Griesinger, C., Otting, G., Wüthrich, K., and Ernst, R. R. (1988) *J. Am. Chem. Soc.* **110,** 7870–7872
20. Rance, M., Sorenson, D. W., Bodenhausen, G., Wagner, G., Ernst, R. R., and Wüthrich, K. (1987) *Biochem. Biophys. Res. Commun.* **117,** 479–485
21. Mueller, L. (1987) *J. Magn. Reson.* **72,** 191–196
22. Güntert, P., and Wüthrich, K. (1992) *J. Magn. Reson.* **96,** 403–407
23. Havel, T. F. (1991) *Prog. Biophys. Mol. Biol.* **56,** 43–78
24. Dauber-Osguthorpe, P., Roberts, V. A., Osguthorpe, D. J., Wolff, J., Genest, M., and Hagler, A. T. (1988) *Proteins Struct. Funct. Genet.* **4,** 31–47
25. Borgias, B. A., and James, T. L. (1989) *Methods Enzymol.* **176,** 169–183
26. Nilges, M., Clore, G. M., and Gronenborn, A. M. (1988) *FEBS Lett.* **239,** 129–136
27. Thomas, P. D., Basus, V. J., and James, T. L. (1991) *Proc. Natl. Acad. Sci. U. S. A.* **88,** 1237–1241
28. Keepers, J. W., and James, T. L. (1984) *J. Magn. Reson.* **57,** 404–426
29. Laskowski, R. A., MacArthur, M. W., Moss, D. S., and Thornton, J. M. (1993) *J. Appl. Crystallogr.* **26,** 283–291
30. Nicholls, A., Sharp, K. A., and Honig, B. (1991) *Proteins Struct. Funct. Genet.* **11,** 281–296
31. Billeter, M., Braun, W., and Wüthrich, K. (1982) *J. Mol. Biol.* **155,** 321–346
32. Wishart, D. S., and Sykes, B. D. (1994) *Methods Enzymol.* **239,** 363–392
33. Sugiyama, N., Marchot, P., Kawanishi, C., Osaka, H., Molles, B., Sine, S. M., and Taylor, P. (1998) *Mol. Pharamacol.* **53,** 787–794
34. Chiara, D. C., and Cohen, J. B. (1997) *J. Biol. Chem.* **272,** 32940–32950
35. Ma, J. C., and Dougherty, D. A. (1997) *Chem. Rev.* **97,** 1303–1324
36. Hucho, F., Tsetlin, V. I., and Machold, J. (1996) *Eur. J. Biochem.* **239,** 539–557
37. Sine, S. M. (1993) *Proc. Natl. Acad. Sci. U. S. A.* **90,** 9436–9440
38. Sine, S. M., and Claudio, T. (1991) *J. Biol. Chem.* **266,** 19369–19377
39. Pedersen, S. E., and Cohen, J. B. (1990) *Proc. Natl. Acad. Sci. U. S. A.* **87,** 2785–2589
40. Sine, S. M., Kreienkamp, H.-J., Bren, N., Maeda, R., and Taylor, P. (1995) *Neuron* **15,** 205–211
41. Luetje, C. W., and Patrick, J. (1991) *J. Neurosci.* **11,** 837–845
42. Harvey, S. C., McIntosh, J. M., Cartier, G. E., Maddox, F. N., and Luetje, C. W. (1997) *Mol. Pharmacol.* **51,** 336–342